# Collective migration of human osteoblasts in direct current electric field

**Jonathan Edward Dawson**[1*], **Tina Sellmann**[2], **Katrin Porath**[2], **Rainer Bader**[3,4], **Ursula van Rienen**[1,3,5], **Revathi Appali**[1,5], **Rüdiger Köhling**[2,5,6]

***For correspondence:** jonathan.dawson2@uni-rostock.de

**Present address:** [§]Institute of General Electrical Engineering, University of Rostock, Rostock, Germany

[1]Institute of General Electrical Engineering, University of Rostock, Rostock, Germany ; [2]Oscar-Langendorff-Institute of Physiology, Rostock University Medical Center, Rostock, Germany; [3]Department of Life, Light and Matter, Interdisciplinary Faculty, University of Rostock, Rostock, Germany; [4]Biomechanics and Implant Research Lab, Department of Orthopedics, Rostock University Medical Center, Rostock, Germany; [5]Department of Ageing of Individuals and Society, Interdisciplinary Faculty, University of Rostock, Rostock, Germany; [6]Center for Translational Neuroscience Research, Rostock University Medical Center, Rostock, Germany

**Abstract** Under both physiological (development, regeneration) and pathological conditions (cancer metastasis), cells migrate while sensing environmental cues in the form of physical, chemical or electrical gradients. Although it is known that osteoblasts respond to exogenous electric fields, the underlying mechanism of electrotactic collective movement of human osteoblasts is unclear. Theoretical approaches to study electrotactic cell migration until now mainly used reaction-diffusion models, and did not consider the affect of electric field on single-cell motility, or incorporate spatially dependent cell-to-cell interactions. Here, we present a computational model that takes into account cell interactions and describes cell migration in direct current electric field. We compare this model with *in vitro* experiments, in which human primary osteoblasts are exposed to direct current electric field of varying field strength. Our results show that cell-cell interactions and fluctuations in the migration direction together leads to anode-directed collective migration of osteoblasts.

## Introduction

The response of the cell to its sensory inputs plays a crucial role in many biological processes such as embryonic development, tissue formation/regeneration and wound healing. One of the crucial common reactions of cells is their directed motility, where cells alter their motion in response to

external stimuli. Generally, such stimuli are considered to consist of chemical (chemotaxis) or mechanical (adhesion and substrate contact; haptotaxis) mechanisms, as well as of temperature gradients (thermotaxis) or electric fields (electrotaxis) ***Simpson et al.*** (***2017***), ***Piotrowski-Daspit*** (***2016***) ***Lara Rodriguez and Schneider*** (***2013***), ***Wu and Lin*** (***2011***); ***Zajdel et al.*** (***2020***). The latter, electrotaxis, also termed galvanotaxis, is increasingly studied in particular in keratinocytes and fibroblasts, since it may provide a promising strategy to foster skin wound healing ***Liang et al.*** (***2020***), ***Cho et al.*** (***2018***), ***Lin et al.*** (***2017***), ***Tai et al.*** (***2009***), ***Saltukoglu et al.*** (***2015***). In this context, several groups aimed to clarify the nature of the electric field sensor. One possible candidate of such a sensor is the outer, negatively charged glycocalyx, which also is responsible for adhesive behaviour ***Hart and Palisano*** (***2017***). Other studies point to an important role of lipid rafts: their redistribution and clustering appear to be responsible for electrical field sensing in fibroblasts, mesenchymal stem cells, and adenocarcinoma cells ***Lin et al.*** (***2017***), but also in corneal epithelial cells ***Zhao et al.*** (***2002***). In most of these cells, the orientation seems to be cathodal (e.g. in fibroblasts and mesenchymal stem and corneal epithelial cells ***Lin et al.*** (***2017***) ***Zhao et al.*** (***2002***)). However, this does not apply to all cell types: adenocarcinoma cells, but also bone marrow mesenchymal stem cells, show the opposite orientation, i.e. anodal ***Lin et al.*** (***2017***); ***Zhao et al.*** (***2011***). Also the downstream signalling apparently is differential; in the various studies, Rho and PI3K ***Lin et al.*** (***2017***), EGF and ERK1/2 ***Zhao et al.*** (***2002***), or PKG, and again PI3K (this time in dictyostelium ***Sato et al.*** (***2009***), where starvation appears to initiate migratory movement ***Guido et al.*** (***2020***)) were found to be involved. Interestingly, a reversal of directionality was reported for keratinocytes when inhibiting P2Y receptors ***Saltukoglu et al.*** (***2015***). We recently reported that store-operated calcium channels are pivotal for electrotaxis in human osteoblasts ***Rohde et al.*** (***2019***), which interestingly migrate to the anode. Thus, both electrotaxis as such, as well as the polarity, seem to be dependent on a variety of factors, such as cell type, environment, possibly age and ontogenetic stage, all of which should influence signalling pathway equipment.

One of the factors that has not found much consideration so far: *In vivo*, electrotactic cell migration involves not only singular, but many cells, for example in a tissue, which collectively respond to either endogenous or exogenous electric fields. Such an electric field-dependent collective cell migration raises the question in which way electric field on the one hand, and neighbour-cell behaviour on the other (both close-range limited by finite volume, and intermediate governed by group orientational alignment) interact to generate a final migration vector. In previous modeling studies, mainly reaction-diffusion based models were used ***Gruler and Nuccitelli*** (***2000***), ***Schienbein and Gruler*** (***1993***), in some cases including interaction between electrical field and chemoattractant ***Vanegas-Acosta et al.*** (***2012***), ***Wu and Lin*** (***2011***). The focus of these approaches was on cell migration mainly at the mean-field level and did not resolve the processes at the level of a single cell. Thus, cell-cell interactions as possible determining factors for cell migration direction and speed have not been modeled so far. Cell-cell communication establishes a network which gives rise to many interesting behaviours, such as non-linear collective response, as observed in quorum sensing, a type of bacterial cell-cell communication ***Waters and Bassler*** (***2005***); ***Thurley et al.*** (***2018***). Quantitative studies have shown that collective cell migration in epithelial structures is an emergent phenomenon, which cannot be explained without taking into account cell-cell interactions

***Barton et al.*** (***2017***); ***Henkes et al.*** (***2020***). A specific class of agent-based model that takes into account interactions between individual active particles during migration in continuous space are the self-propelled particle models, which were developed to understand flocking phenomena and show that under some conditions transitions can be observed where collective effects give rise to a common motility pattern ***Bittig et al.*** (***2010***); ***Vicsek et al.*** (***1995***); ***Bhattacharya and Vicsek*** (***2010***). Self-propelled particle based models have been widely used to study collective behaviour in cell migration in tissues ***Szabó et al.*** (***2006***); ***Trepat et al.*** (***2009***). Self-propelled voronoi model, a hybrid of self-propelled particle model and vertex model, that links active cell mechanics with cell shape and cell motility predicts a liquid-solid transition in confluent tissues, where cell-cell interactions, among others, play a key role ***Bi et al.*** (***2016***), ***Merkel and Manning*** (***2017***); ***Henkes et al.*** (***2020***). While inclusion of cell-cell interactions in models seem to be natural in the case of high-density tissue culture, where cells adhere to each other and thus exert a pulling force on the neighboring cells, for examples in epithelial wound healing ***Brugués et al.*** (***2014***), the rules governing such an interaction in a system of isolated cells, such as *in vitro* cell culture, remains ambiguous. To our knowledge, to date no computational model has taken into account individual cell interactions to study migration of cells stimulated by external electric field. Here, we propose a novel data-driven model for collective dynamics of cells stimulated by direct current (DC) electric field. By re-analysing data on individual cell basis from our recent study on osteoblast migration mechanisms in DC electric field ***Rohde et al.*** (***2019***), we test the hypothesis that cell-cell interactions shape the total vector.

## Results

### In vitro DC stimulation of human osteoblasts

In the experimental part of this study, we exposed human osteoblasts to DC electric fields for 7 hours (h) at different stimulation strengths and matched each of these experiments with a sham-stimulated, control group treated identically, save the DC stimulation. For the analysis of the migration behaviour, we selected adherent cells in the stimulation chambers which could be identified clearly at starting and end points of the experiment, and did not form clusters precluding the outlining of their boundaries (Figure 1 A-C). Using photographs of several fields of vision in each chamber, 1-4 cells could be traced in this way per field of vision position, totalling n=177 cells (sham stimulation), as well as n=34 cells (at 160 V/m), n=35 cells (at 300 V/m), n=26 (at 360 V/m), n=43 (at 425 V/m) and n=33 (at 436 V/m). As one can notice in the original photographs of one typical cell from the experiment using 436 V/m stimulation, the cells move (in this case anodally), and at the same time change their shape within the 7 h stimulation (Figure 1 A-C). While we did not analyse shape changes any further in this study, we took them into consideration by using centroids of the cells (blue dots in Figure 1 C) as markers to determine the net movement.

Comparing cell migration velocities (plotted as sectors of polar plots) without stimulation (Figure 1 D), to those with weak (160 V/m; Figure 1 E) or strong stimulation (436 V/m; Figure 1 F), one can appreciate that the directionality of migration shifts from random, covering all sectors of the plot (Figure 1 D) to exclusively anodal, covering only the anodal sectors (Figure 1 F), with increasing field strength. At the same time, also the speed of the cells appears to shift from lower speeds

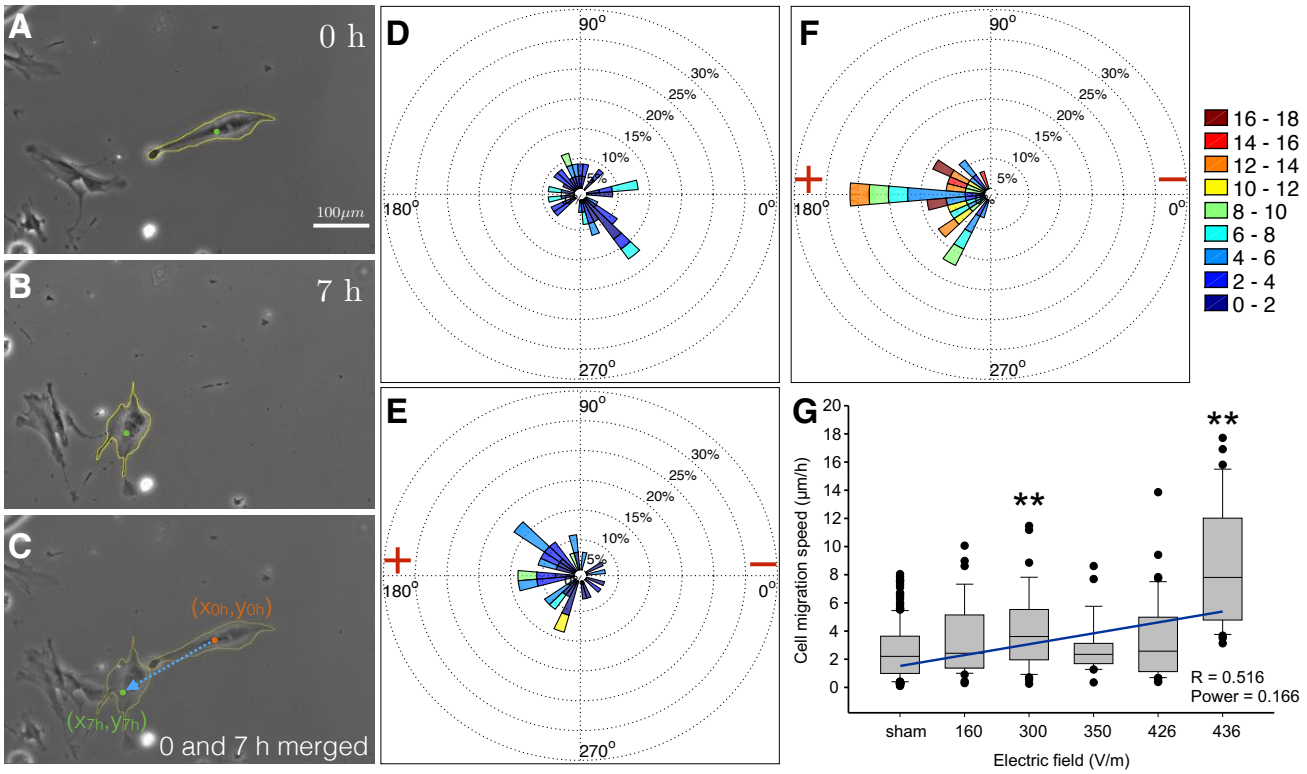


**Figure 1. Single-cell analysis of migration of osteoblasts in a DC electric field. A-C** Photomicrographs of osteoblasts in stimulating chamber. Cells boundaries were manually outlined as depicted (yellow coastline). (**A**) denotes the time point before stimulation. (**B**) shows the position of the same cells after 7h DC-stimulation (436 V/m). (**C**) demonstrates the overlay of **A** and **B**. Blue arrow: displacement of cell centroid. (**D-F**) Polar plots showing the velocity of cell migration in the cases of sham (**D**), 160 V/m, (**E**), and 436 V (**F**) DC stimulation. Width of sectors within these polar plots corresponds to 10° each; data of cells migrating within each 10° sector are cumulated. Speed range is color coded (in μm/h) as shown in the insets. The relative sector lengths denote the percentage of cells migrating at a certain speed range. (**G**) Box and whisker plot of medians (horizontal lines) of cell migration speed vs. electric field strength. Whiskers denote 25-75 percentiles of data distribution. Dots show data lying outside these percentiles. Numbers of cells for each experiment are: 177, 34, 35, 26, 43, 33 for sham, and 160, 300, 360, 426 and 436 V/m, respectively. Both at 300 V/m, and at the maximum strength of 436 V/m, the speed is significantly higher than under all other conditions ($p<0.001$; asterisks, ANOVA on ranks, all-pairwise comparisons using Dunn's test). Speed thus correlates weakly with applied electric field, showing a regression (blue line) of R = 0.516, albeit at low power 0f 0.166.

with a maximum of 8-10 μm/h (green hues in Figure 1 D corresponding to $\sim 2.5\ \%$ of the cells) to a maximum of 16-18 μm/h (red sectors in Figure 1 F corresponding to $\sim 12\ \%$ of the cells).

To address the question of a possible correlation of speed and field strength, we quantified the cell migration speed of all cells in all experiments under different stimulation strengths. As shown in Figure 1 G, migration speed under DC-stimulation is significantly different from sham stimulation conditions only at 300 V/m and 436 V/m ($p< 0.001$, ANOVA on ranks with Dunn's all-pairwise comparisons). Considering all values and calculating a linear regression (blue line in Figure 1 G), there is thus a weak correlation between field strength and migration speed, with a regression coefficient of $R = 0.516$.

## Modeling electrotactic collective osteoblast cell migration

We describe the *in vitro* motility behaviour of individual cells that are subject to external DC electric field. The main components of our model are (i) the ability of the cells to interact with the other cells, and, (ii) the ability of the cells to interact with the external electric field. The cell-cell interaction involves two types of forces: short-range repulsive forces, and the alignment of the direction of motion with the cells' local neighbours. The force at the short distances, through soft-core repulsion, ensures that cells do not overlap. We also include in our model the influence of each cell's local neighbours on the direction of its migration. Such cell-to-cell interactions are certainly playing a role in high-density tissue culture via cell-cell contacts. However, since mechanical or signalling cues are at least conceivable also in 2D cell cultures without direct cell contacts, we introduce this factor in the model to study the possible role of such interactions in our experiments. Finally, we also consider the interaction of cells with the applied DC electric field.

### The cell

Each cell is modeled as a circular disk of radius $R$ which can migrate in two spatial dimensions with an active speed of $v_0$. The state of each cell $i$ is characterised at time $t$ by its position $\mathbf{r}_i^t$, described through the coordinates $(x_i^t, y_i^t)$, and its migration velocity $\boldsymbol{v}_i^t = v_0 \boldsymbol{s}_i^t$, where, $v_0$ is the cell migration speed and $\boldsymbol{s}_i^t = (\cos\theta_i^t, \sin\theta_i^t)$ is the unit vector representing the direction of migration, with $\theta$ being the angle that the cell makes with the horizontal axis of the laboratory frame. The direction $\theta$ that each cell takes at any consecutive time depends not only on its direction of motion in the immediately preceding time, but also on the forces acting on the cell. The total force acting on the cell $i$ results from cell-cell interactions and cell interaction with the applied DC electric field, These forces are discussed in more detail in the following sections.

### Cell-cell interactions

We consider two types of cell-cell interactions in our model. The cell-cell interaction due to finite-volume exclusion and the cell-cell interaction resulting from cell orientational alignment with its neighbours. Each cell is assumed to occupy a finite area in the cell culture medium in which it is placed. To avoid cell overlaps, we include repulsive force $\boldsymbol{K}_{ij}$ that is proportional to the degree of overlap between two cells and is given by,

$$\boldsymbol{K}_{ij} = k(2R - r_{ij})\hat{r}_{ij} \tag{1}$$

with, $\boldsymbol{r}_{ij} = \boldsymbol{r}_i - \boldsymbol{r}_j = \hat{\boldsymbol{r}}_{ij} r_{ij}$ and $k$ a force constant. $r_{ij}$ is the euclidean distance between two cells $i$ and $j$ and is calculated as $\sqrt{(x_i - x_j)^2 + (y_i - y_j)^2}$. The total repulsive force acting on cell $i$ at time $t$, denoted by $\boldsymbol{F}_i^t$ is,

$$\boldsymbol{F}_i^t = \sum_{|\boldsymbol{r}_j^t - \boldsymbol{r}_i^t| < 2R} \boldsymbol{K}_{ij}. \tag{2}$$

The directional alignment of cells with its proximal neighbours is given by,

$$\theta_i^t = Arg\Big[\sum_{|\boldsymbol{r}_i^t - \boldsymbol{r}_j^t| < r_a} s_j^t\Big] + \eta\xi_i^t \tag{3}$$

and is only hampered by an angular white noise uniformly distributed in $[-\pi, \pi]$ with $\langle \xi_i^t \rangle = 0$ and $\langle \xi_i^t \xi_j^{t'} \rangle \sim \delta_{ij}\delta_{tt'}$ and whose strength is given by $\eta$. The function $Arg$ in Equation 3 returns the angle

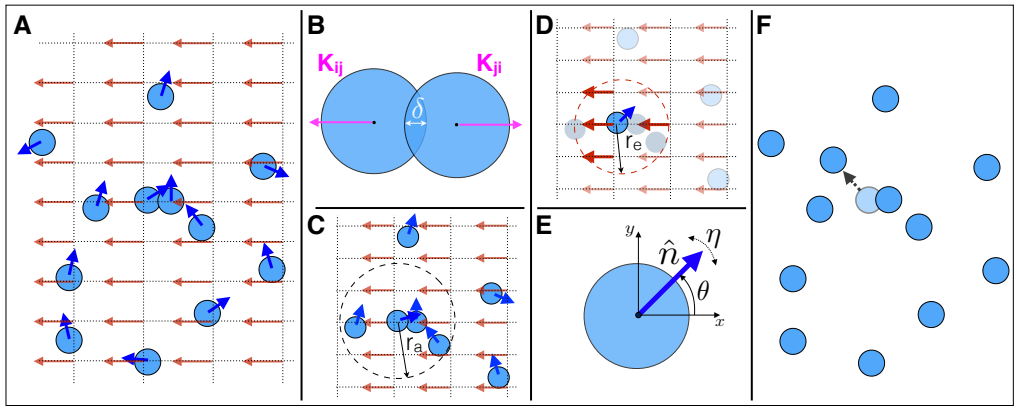


**Figure 2. Theoretical model for cell migration in a DC electric field. (A)** Osteoblasts in the cell culture chamber exposed to the DC electric field, are modelled as active particles (light blue colored disks) of radius $R$ and velocity $v_i$ ($i$ is the index of the cell). The dark blue colored arrows laid over the circular disks are the cell velocity unit vectors $\hat{n}$. The model takes into account both cell-cell and cell-electric field interactions. These interactions can influence the cell velocity. Cell-cell interactions involve finite-volume exclusion and migration orientation alignment. **(B)** When two cells overlap, each cell $i$ experiences a displacing force $K_{ij}$ from its neighboring cell $j$, where $i$ and $j$ are the cell indices. The magnitude of such a force is linearly proportional to the degree of overlap $\delta$. The total force experienced by the cell from all its overlapping **(C)** The migration direction of a cell can be influenced by its neighbouring cells located within the radius $r_a$, taken from the cell's center. Such an interaction re-orients the migration direction of a cell to the average direction of migration of neighbouring cells. **(D)** Each individual cell also experiences the force due to the electric field. The electric field is defined on discrete grid points in the two-dimensional space in which the cells move. A cell experiences the average force from the electric field at all the grid points that lie within the radius $r_e$, also taken from the cell's center. The net angle $\theta$ of cells alignment results from the cumulative effect of the cellular interactions described in **(B-D)**. **(E)** The limited precision in cellular sensing of directional alignment is captured by an angular white noise term whose strength is given by $\eta$. **(F)** As a result of these interactions, the model at each time step calculates and updates the position of each cell (shown by dotted arrow for the cell under consideration) for the next time step.

defining the orientation of the average vector $\sum_{|\boldsymbol{r}_i^t - \boldsymbol{r}_j^t| < r_a} s_j^t$, where the sum extends only to those cells which are within the interaction radius $r_a$ of cell $i$.

## Cell-electric field interaction

The electric field is defined on a regular square lattice underlying the domain in which the cells are migrating. Each grid point is specified by coordinates $(p, q)$. The electric field at the grid point located at $(p_k, q_k)$ is characterised by the unit vector $\boldsymbol{d}_k = (\cos\Theta_k, \sin\Theta_k)$ and the electric field amplitude $E_0$, which corresponds to the electric field strength of experimental electrical stimulations. $\Theta_k$ is the angle that the electric field vector at $(p_k, q_k)$ makes with the horizontal. Cell $i$ experiences an effective electric field which is the average of the electric field on all the grid points that lie in the region within the radius $r_e$ of cell $i$. The net electrical force experienced by cell $i$ is proportional to the net electric field strength and is given by,

$$\boldsymbol{D}_i^t = E_i^{\text{net}}(\cos\Theta_i^{\text{net}}, \sin_i\Theta^{\text{net}}) \tag{4}$$

where, $\Theta_i^{\text{net}}$ and $E_i^{\text{net}}$ are the mean orientation and the mean strength of the electric field $\boldsymbol{E}_i^{net}$ sensed by the cell at the location $(x_i, y_i)$.

**Table 1.** List of all the model parameters, their notation, description and value (dimensionless).

| Parameter | Description | Value |
|---|---|---|
| $R$ | cell radius | 1 |
| $v_0$ | active cell speed | 1 |
| $k$ | repulsive force constant | 1 |
| $\nu$ | friction factor | 0.1 |
| $\eta$ | noise strength | 0.05 |
| $r_a$ | distance over which orientation alignment occurs | 2 |
| $r_e$ | distance up to which electric field is sensed by the cell | 2 |
| $\mu$ | electrical mobility of cell | 0.04 |

After calculating all the interactions, including the cell neighbor orientation alignment, the position of each cell is updated at the end of each time step by the following scheme:

$$\boldsymbol{r}_i^{t+1} = \boldsymbol{r}_i^t + \nu(\boldsymbol{v}_i^t + \boldsymbol{F}_i^t + \mu \boldsymbol{D}_i^t) \tag{5}$$

where, $\nu$ is a friction factor that is associated with the cell substrate interaction and $\mu$ is the cell mobility in the presence of external electric field.

## Simulation details

We simulate the motility behaviour of $N = 35$ cells, since in our experiments there are approximately 30-40 cells in a single field of view. Cells are initially randomly distributed in a circular region within the spatial domain representing the stimulation chamber. In our simulations we also study the effects of higher initial cell densities on cell migration in DC electric field. Osteoblast cells are roughly 100 $\mu m$ in diameter considering all cells extensions, and we use this to define the cell radius $R$, which is one length unit in our simulations. The cell radius $R$ is assumed to be the basic length scale in these simulations. The active speed of cells is $0.1R$ per time step. Time steps are seperated by $\Delta t$ which is set to 1. The time parameters in the simulations are scaled such that the speed of cells in the case of no electric field corresponds to the average speed of cells in the experimental case of unstimulated sham, which is $\sim 3\mu\mathrm{m/h}$. At the start of each simulation, we specify the initial positions $x_i^0, y_i^0$ of each cell $i$ and assign their initial speed $v_i^0$ as well as the orientation $\theta_i$, which is distributed randomly in the range [0,2$\pi$]. At each time step for each cell we identify cells which are less than a distance of $2R$ apart. From this we calculate the force due to volume exclusion acting on each cell from its neighboring cells, as given by Equation 1 and 2. We also determine all the grid points of the underlying grid, on which the electric field is defined, that are within the radius of $r_e$ of each cell and calculate the mean electric field. This constitutes the net force due to the electric field $\boldsymbol{D}_i$ acting on each cell $i$, as given by Equation 4. Experiments show that the cell migration is anode-directed. We incorporate this into our model by assigning a polarity to the mean electrical force, experienced by the cell, that is opposite to the applied electric field, i.e $\boldsymbol{D}_i = -\boldsymbol{E}_i^{net}$. In addition, we also determine for each cell all its neighboring cells that are located within the radius $r_a$, and calculate the mean orientation of all those cells. Each cells' orientation is updated by its mean

orientation, to which a weak noise $\eta = 0.05$ is added, as given by Equation 3. Finally, the positions of each individual cell is then updated using the Equation 5.

## Migratory behaviour of osteoblasts in DC electrical field

To study the influence of externally applied DC electrical field on the migratory behaviour of human osteoblast we simulated N=35 migrating cells with and without DC electrical stimulation for 130 time steps. The parameters of the model and their values used in these simulations are listed in Table 1. Due to random initial conditions and stochastic angular fluctuations in the simulations, we have verified through multiple runs of the simulations that our results are qualitatively invariant, Figure 3–Figure supplement 1. We use periodic boundary conditions, to reflect the experimental conditions in which cells are placed in the center, and thus far from the boundaries, of the stimulation chamber. Figure 3 left column shows the positions of all cells at the final time step, in the case of no electrical stimulation, Figure 3 A, and in the case of DC electrical stimulation with field amplitudes of 0.36 and 1, Figure 3 B and C, respectively. Electric field amplitude of magnitude 1 in simulations corresponds to the maximum field strength of electrical stimulation in experiments, i.e., 436 V/m, Figure 1 G. Figure 3 D-F (upper row) shows the individual cell trajectories at each time step in the case of no electrical stimulation, Figure 3 D, and in the case of electrical stimulation with different field amplitudes of 0.36 and 1, Figure 3 E and F, respectively. The velocity of cell migration, calculated from the initial and the final time step, is shown in Figure 3 G-I as polar plots for the case without electrical stimulation, Figure 3 G, and with electrical stimulation of different field amplitudes, i.e, 0.36 and 1, Figure 3 H and I, respectively. Each polar plot shown in Figure 3 G-I, is the cumulate of 10 separate runs of the simulation. Initial velocity of each cell and the noise in cell velocity at each time step are random, this renders robustness to the polar plot distributions.

In the absence of electrical stimulation the cells move, as expected, in all directions, Figure 3 A. Trajectories of individual cells show that, over time, all cells collectively explore the space homogeneously, Figure 3 B, a feature which is also reflected in the polar plots, which are constructed, similar to the experiments, based only on the initial and final time steps Figure 3 G. The mean cell speed in this case is $\sim 3\mu$m/h. However, when DC electrical field of amplitude 0.36, which corresponds to 160 V/m, is applied, cells start exhibiting a directional migration towards the anode 3 B. Individual cell trajectory plot shows that although the final position of the majority of the cells is towards the anode, few cells still migrate towards the cathode, albeit much shorter distances than the anodally migrated cells, 3 E. The polar plot, showing velocity of cell migration, clearly shows the modulation of the orientation of migration by external field, 3 H. Following the trajectories of individual cells also shows that cell migration is not instantaneously switched in the direction of anode. Cells respond to the applied electrical field by gradually changing their directionality of migration. Initially most of the cells move orthogonal to the applied field and then, at later times, gradually turn towards the anode. This delayed response in eventual anode directed motility of cells is because the force due to the electric field $\mu E_0$ is much weaker than the active cell migration speed $v_0$. When the strength of the electric field $E_0$ is increased to 1, the directionality of cell migration shows a stronger re-orientation towards the anode, 3 C. Cell migration in this case shows a much faster re-orientation and much persistent motion towards anode 3 (F). Figure 3 I shows that not

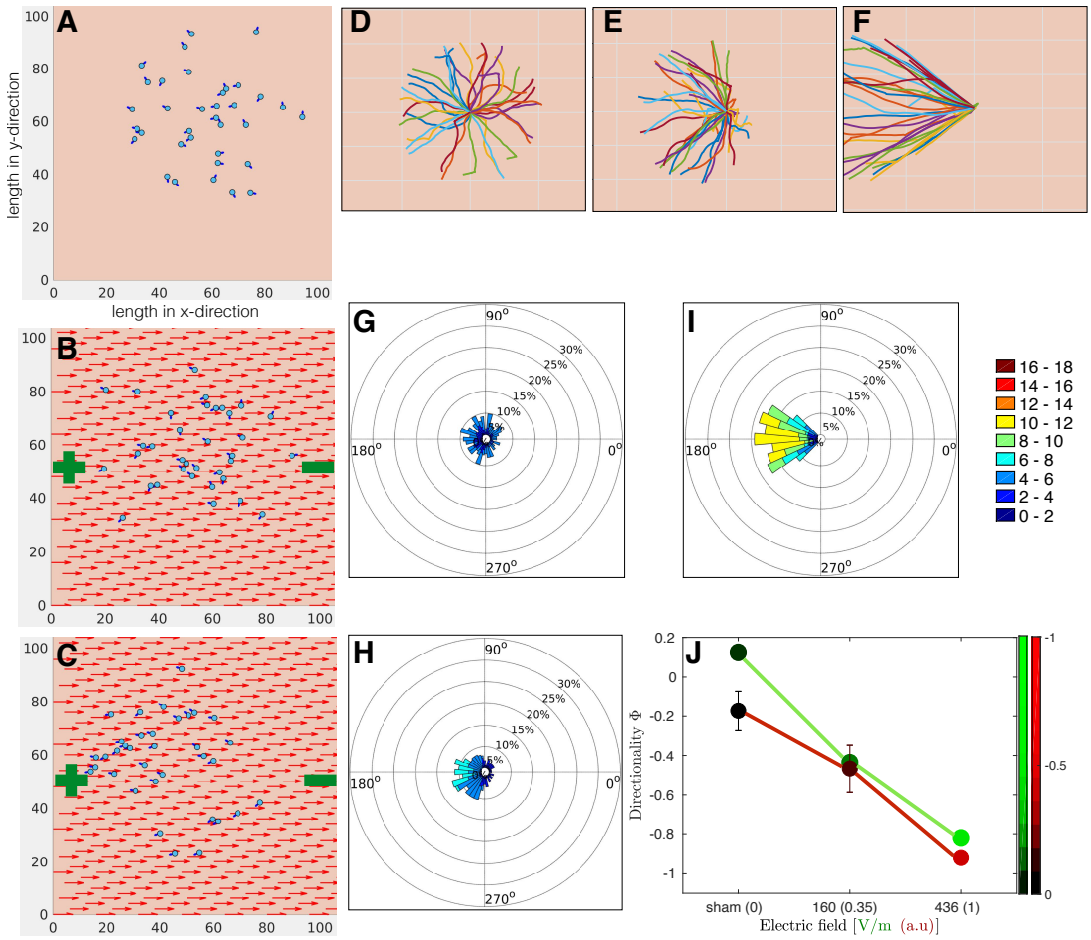


**Figure 3. Simulation of cell migration model in DC electrical field.** Each simulation consists of 35 cells initially randomly distributed in a circular region around the center of the domain of size 120×120. Osteoblasts are modelled as light blue colored circular disks of radius R=1 and randomly oriented initial migration velocity, shown by dark blue arrows. The cells have an active speed that propels them a distance of 0.1R per unit time. In these simulations, $r_a = 2$, which results in a situation where direct cell contact not only leads to repulsion forces due to volume exclusion, but also an alignment force leading to common reorientation of the movement direction of the individual cells. In addition, the noise strength $\eta = 0.05$, results in directionality fluctuations in the range $[-8°, 8°]$. The model is simulated for 130 time steps. (**A-C**) Final positions of individual cells in the case of no DC electric field (**A**), with DC electric field of strength 0.36 (**B**) and 1 (**C**),respectively. Electric field strength of 1 in simulations corresponds to the maximum electric field strength of 436 V/m in experiments. The polarity of the DC electric field is shown by green colored plus and minus symbols in (**B**) and (**C**). (**D-F**) Trajectories of individual cells corresponding to the three cases shown in (**A-C**), respectively. Cell positions are adjusted such that all the trajectories originate from $x = 0$ and $y = 0$ at $t = 0$. (**G-I**) Polar plots showing the velocity of cell migration taking into account only the initial and the final time step, corresponding to the three cases shown in (**A-C**), respectively. Each polar plot is a cumulate of data from 10 separate simulation runs, where each simulation consists of 35 cells. Simulation cell speed in the case of no electrical stimulation are scaled to the mean cell speed of experimental sham, i.e $\sim 3$ $\mu$m/h. This constant rescaling factor is then multiplied to individual cell velocities from simulation in electrical stimulation cases. (**J**) Directionality order parameter $\Phi$ obtained from simulations (dots in shades of red connected by red lines) and experiments (dots in shades of green connected by green lines) corresponding to the three different cases shown in (**A-C**). The electric field strength in simulations is shown in arbitrary units (a.u), where 1 (in brackets) corresponds to maximum strength of 436 V/m in experiments. Different shades of the two colors (red and green) correspond to the magnitude of the directionality as shown in their respective colorbar. Each value of directionality obtained from simulations is the average of 10 separate simulation runs, where each simulation consists of 35 cells. Error bars in simulation data show the standard deviation in $\Phi$.

**Figure 3–Figure supplement 1.** Individual cell trajectories for multiple simulation runs.

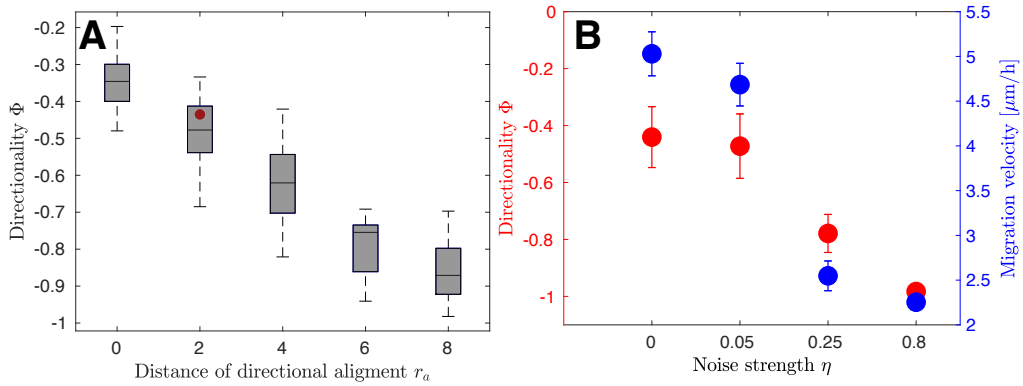


**Figure 4. Influence of directional alignment and noise strength on cell migration.** Parameter sweep was performed to study the influence of directional alignment and noise strength on the directionality of migration in the case of electrical stimulation of strength 0.35, which corresponds to 160 V/m in experiments. Each simulation data point is an average of 10 independent simulation runs. (**A**) Box and whisker plot of medians (horizontal lines) of directionality of migration $\Phi$ vs. distance of directional alignment $r_a$. The values of all other parameters, except $r_a$, are as mentioned in Table 1. Cells show higher directedness $\Phi$ in their migration towards anode with increasing distance $r_a$ over which directional alignment occurs. The red dot is the experimental value for the directionality in the case of electrical stimulation of strength 160 V/m. Whiskers denote 25-75 percentiles of data distribution. (p<0.001; statistical significance was estimated by performing one-way ANOVA analysis using MATLAB 2018b, The MathWorks, Natick, 2018). $\Phi = -1$ corresponds to fully directed movement towards the anode, which is located at 180° in Figure 1 D-F and Figure 3 G-I. **(B)** Directionality order parameter $\Phi$ (red) and migration velocity (blue) vs. noise strength $\eta$. The values of all other parameters, except $\eta$, are as mentioned in Table 1. Increasing noise strength leads to higher directedness in cell movement towards the anode $\Phi \sim -1$. However, for the same values of noise strength, migration velocity decreases with increasing noise strength. Error bars show the standard deviation in the directionality and the migration velocity for different values of noise strength obtained from simulations.

only the direction of the motion is influenced by increasing field strength, but also the velocity of the cell migration. The maximum cell speed in this case even reaches up to 10-12 $\mu$m/h, Figure 3 I. To better quantify the changes in the collective cell migratory behaviour we calculate, in both experiments and simulations, the directionality order parameter $\Phi$, which reflects how well cell movements have aligned with the electric field and directed towards the anode, and is given by,

$$\Phi = \frac{1}{N} \sum_i \cos(\theta_i) \tag{6}$$

where, $N$ is the total number of cells and the sum is over the cosine of migration direction of individual cells $\theta_i$. $\Phi$ can vary between 1 (towards cathode) and -1 (towards anode) and $\Phi \simeq 0$ corresponds to random cell movement. Our results show that for the listed choice of parameters, the directionality order parameter $\Phi$ obtained from the model simulation matches very closely with the experiments, Figure 3 J.

Our results shown in Figure 3 reproduce the following experimental observations (i) in the absence of electrical stimulation, which corresponds to the experimental sham case, directional migration of cells is not observed and cells collectively move in all directions, (ii) alignment of the directionality of cell migration depends on the strength of the applied electrical field, (iii) average cell velocity increases with the field strength.

### Influence of direction alignment and noise on cell migration

In our model the collective behaviour results from the directional alignment of individual cells with each other. This is controlled by the model parameter $r_a$, which is the distance over which the cell aligns its direction of migration with its neighbors, and $\eta$, which is the strength of the fluctuation in the direction of migration of individual cell. In the simulation results discussed in the preceding section, Figure 3, we considered $r_a = 2R$, i.e the orientation alignment occurs only when cells touch each other. In order to understand how the two model parameters $r_a$ and $\eta$ affect the migratory behaviour of electrically stimulated osteoblast cells, we perform a parameter sweep study of cell migration with fixed electrical stimulation of strength 0.36 (which corresponds to 160 V/m in experiments) and different values of $r_a$ and $\eta$ as shown in Figure 4A and B. The values of all the other parameters are as mentioned in Table 1. Our results show that, even in the case of weak electrical stimulation, which corresponds to 160 V/m in experiments, with increasing $r_a$ the cells move in a more directed manner towards the anode, i.e $\Phi$ approaches the value of $-1$ Figure 4A. Cell movement also shows higher directedness with increasing noise strength $\eta$, which is unexpected, Figure 4B. On the contrary, the cell migration velocity decreases with increasing noise strength, Figure 4B. Taken together these results suggest that the parameters $r_a$ and $\eta$ can significantly alter the dynamics of cell migration and give rise to collective electrotactic motion of osteoblast cells.

## Discussion

The migration of osteoblasts, which plays a key role in bone regeneration, can be modulated by external electrical stimulation ***Ferrier et al.*** (***1986***). This offers an attractive approach towards building electrically active implants for effective tissue regeneration ***Hiemer et al.*** (***2016***); ***Kaivosoja et al.*** (***2015***); ***Brighton et al.*** (***1985***). In the present paper, we presented a computational model to study (i) the migratory behaviour of osteoblasts, and, (ii) the consequences of the application of external electrical field on their migration. The model was used to study the collective behaviour of many cells in *in vitro* experiments where primary human osteoblasts placed in electrotaxis chamber were stimulated by DC electric field. For this purpose, we re-analysed the galvanotactic migration of human osteoblasts exposed to DC-electric field stimulation at different field strengths from a previous study published in ***Rohde et al.*** (***2019***), now using single-cell rather than clustered data. As observed in our previous paper ***Rohde et al.*** (***2019***), we confirmed that field exposition leads to migratory directionality towards the anode, and elucidate that the migratory speed distribution ranges from 2-18 μm/h, with significantly higher speeds of migration than unstimulated cells at DC-field strengths of 300 and 436 V/m. Using this single-cell analysis approach, beyond our initial findings in the cited paper using pooled data (i.e. stimulated vs. unstimulated only), we show that the directionality thus actually significantly depends on the field strength, with random migration without stimulation, $\sim$ 65% anodal migration at low (160 V/m) and exclusively anodal migration at highest field strength (436 V/m). Our detailed cell-by-cell analysis analysis also shows that, although directionality of cell migration clearly correlates with the strength of the applied electric field, there is only a weak correlation of migratory speed and electric field strength, a correlation which could not be seen in the pooled analysis of our previous paper.

To explain these experimental observations, we modeled each cell as an active agent whose movement is influenced by its own interactions with other cells, external electric field and stochastic switching in the direction of migration. The model takes into account the force experienced by the cell due to the applied DC electric field. We also considered two types of inter-cellular interactions: in addition to the nearest neighbor interaction that ensures finite-volume exclusion by penalizing cell overlaps, cells also interact with other cells via a velocity alignment mechanism. Although specific molecular mechanisms underlying these interactions remain unclear, two important questions can be addressed by the current simulation study: (i) Does directionality also depend on interaction among neighbouring migrating cells, and if so, how large is this interaction radius, (ii) Do directionality and migration speed depend on the accuracy of the putative cellular field sensing mechanism, i.e. in which way does a noise factor influence migration directionality and migration speed?

Our results show that the motility behaviour of cells is influenced by the distance over which the cell aligns with its neighbors, stochastic switching in the direction of migration and the strength of applied electric field. The simulations in the present paper closely match the experimentally observed weak correlation between migration speed and the applied electric field, and are more realistic than previously published ones ***Vanegas-Acosta et al.*** (***2012***), which predicted speed ranges from 1.8 to 4.0 μm/s, i.e. nearly tenfold the maximum observed by us. As discussed previously, migration at such high speeds probably finds its limitations in adhesive forces acting on the cells on the one hand, and rate-limiting factors such as actin conformational change being limited by temperature and $Ca^{2+}$ dynamics ***Jacobs et al.*** (***2011***); ***Sich et al.*** (***2010***). We performed a quantitative comparison of the directionality order parameter obtained from simulations with experiments as shown in Figure 3(J), where directionality angles $\Phi$ of experimental values and simulations practically overlap. As the simulation results show, varying $r_a$ from 0 (i.e the case with no inter-cellular interactions) to 8 (i.e. the case with inter-cellular interactions between two cells extending to distances of four cell diameters), the directionality of $\sim$ -0.45 for electrical stimulation of strength 160V/m, as found in our experiments, best matches with a value of $r_a$ of 2. These results suggest that the interactions between cells only in direct contact likely lead to parallel anodal movement. The mechanism of this interaction could be speculated to rely on e.g. osteoblast binding via cadherin, an interaction known to be important for morphogenesis of osteoblasts, and subsequent modulation of actin function ***Stains and Civitelli*** (***2005***); ***Stains et al.*** (***2019***). Long-distance effects, mediated by e.g. molecules secreted from the cells, tension changes within the collagen coating, or distortion of the electric field by the neighbouring cell are, in turn, unlikely to be important for osteoblasts.

Our results also show that stochastic orientational switching can significantly alter cellular electrotactic motility behaviour. In this case, a perfectly directed motion towards the anode is achieved for very high fluctuation strengths, which appears to be counter-intuitive since one would expect that for higher angular fluctuations the accuracy of directional movement aligned with the electric field decreases. Varying $\eta$ in our simulations from 0 to 0.8, the directionality of $\sim$ -0.45 in our experiments is in line only with a very low degree of noise (around 0.05, which corresponds to fluctuations of $\sim$ 10°in the direction of cell migration), but not commensurate with values of $>$ 0.25.

The experimental migration speed found to be in the range of 2 to 12 µm/h would also cover the simulated value of $\sim$ 4.75 µm/h at $\eta = 0.05$. It is, however, conceivable, that other cell types do show more influence of noise (arguably reflecting e.g. less mechanical interactions with the substrate, varying cell shape influences, or different field sensing or signalling mechanisms). What remains to be explained is the seemingly paradoxical result that higher fluctuation levels should lead to higher accuracy in directionality. Our hypothesis would be that higher fluctuation actually raises the probability of cell-to-cell interactions, which in turn will lead to common field alignment. If this hypothesis holds true, such movement would lead to field orientation of cells with higher accuracy but lower speed due to frequent corrective movements. Although experiments clearly are needed to validate this hypothesis, it is interesting to note that at the highest stimulation strength of 436 V/m, those cells which are best aligned to the field and directed towards anode do not belong to the fastest subset of cells (which are, indeed, 10°-30°off the "ideal" orientation; see Figure 1 F). Interestingly, in a different biological system, such noise-induced collective migration has been observed in fish schooling ***Jhawar et al.*** (***2020***).

Our data-driven model presented provides a framework for studying cell migration and elucidating the rules and the role of individual cell interactions, with other cells and with their physical environment. This model may also be relevant to study the influence of cell density and other modes of electrical stimulation, such as alternating current stimulation on cell migration. Our approach could serve as a tool to not only test existing hypotheses of electrotactic cell migration but also predict migratory behaviour under perturbation conditions.

## Methods and Materials

### Experimental Methods

In this study, data on cell migration of human osteoblasts under DC-electrical stimulation were reanalysed using a previous set of experiments ***Rohde et al.*** (***2019***). Cell cultivation and stimulation methods are detailed in this paper, and given in brief below:

### Cell culture

Human osteoblasts were isolated from femoral heads of patients (n = 14) undergoing a total hip replacement. Patients gave consent and the study was approved by the local ethics committee (permit A 2010-10). Osteoblasts were isolated from cancellous bone as previously described ***Lochner et al.*** (***2011***). Isolated cells were cultured in Dulbecco's Modified Eagle Medium (Pan Biotech, Aidenbach, Germany) supplemented with 10%fetal calf serum, 1% amphotericin B, 1% penicillin-streptomycin and 1% hepes- buffer under standard cell culture conditions (5% $CO_2$ and 37°C). Ascorbic acid (50 $\mu$g/ml), $\beta$-glycerophosphate (10 mM), and dexamethasone (100nM) (Sigma Aldrich, St. Louis, MO, US) were added to cell culture medium to maintain osteoblast phenotype. For cell migration experiments cells in passage three were used.

### DC electrical stimulation chamber and experimental procedure

To study migration of osteoblasts in electric fields, we used a two-part stimulation chamber described in ***Rohde et al.*** (***2019***). Before each use, both chamber parts were cleaned with 70% ethanol,

washed with a mild detergent and rinsed extensively with distilled water before steam sterilization. Coverslips (24 × 50 mm) for seeding osteoblast cultures were coated with rat tail collagen (Advanced Biomatrix, San Diego, CA, USA) by incubation of 50 $\mu$m/ml rat tail collagen diluted in sterile 0.1% acetic acid for 1 h. Coverslips were positioned in a groove in the upper chamber part and edges sealed with silicon paste (Korasilone, Obermeier GmbH, Bad Berleburg, Germany). Upper and lower chamber parts were bolted by 12 screws to ensure tight contact and prevent leakage and chambers were exposed to UV light for sterilization. After this sterilisation treatment, remaining solution was aspired and coverslips were washed twice with phosphate buffered saline (Biochrom, Berlin, Germany) before cell seeding. A total of $2 \times 10^3$ osteoblasts were seeded per chamber and cells were allowed to adhere for 30min. Afterwards, coverslips were washed twice with medium to remove non-adherent cells. Chambers were then sealed with a top coverglass, and silicon paste and cells accommodated to chamber overnight. For DC-stimulation, silver/silver chloride electrodes were placed into outer reservoirs separated from cell area to avoid electrochemical reactions within the tissue chamber. Current was conducted to the cell chamber using agar bridges (silicon tubes, length 120mm, inner diameter 5 mm) consisting of 2% agarose (TopVision agarose, ThermoScientific, Waltham, MA, US) in Ringer's solution (Braun, Melsungen, Germany). Current was applied to electrodes for 7 h via crocodile clamps using a DC power supply (Standard Power Pack P25, Biometra, Göttingen, Germany). To maintain constant stimulation, voltage was measured directly at the borders of the cell area (electrode distance 24 mm) using a multimeter (Voltcraft VC220, Conrad Electronic, Wollerau, Switzerland) and adjusted during the experiments. Each of the experiments was conducted with one cell culture being divided to obtain sham stimulation group as control, and a DC-stimulation group for the respective field strength used. Electric field strengths were 160, 300, 360, 426 and 436 V/m.

## Migration analysis

For the analysis, all cells from the sham groups were pooled as one control. Thus, a total of n=177 (sham), 34 (160 V/m), 35 (300 V/m), 26 (360 V/m), 43 (426 V/m) and 33 (436 V/m) cells were analysed. For this, photographs were taken at 8 fields of view evenly distributed over the cell area at beginning (Figure 1A) and end time points (Figure 1B) with a Leica DMI 6000 and LAS X software during the 7-hour stimulation, or sham stimulation, procedure. The pairs of photographs were then aligned manually, and merged, taking external markers as reference points (Figure 1C). To quantify migration within the electric field, segmentation of the cell shape, including cell extensions, was performed manually using Image J software (NIH) for each cell that could be identified in both the time points (see yellow coastlines in Figure 1C), i.e 0 hours and 7 hours after DC stimulation. Using the coordinates of the cell centroid at these two time points, the distance and orientation of migration was calculated for each cell. The migration distance was defined as $d = \sqrt{(X1 - X2)^2 + (Y1 - Y2)^2}$, where $X1, Y1$ and $X2, Y2$ represent the coordinates of the cell centroid at 0 hours and 7 hours after DC stimulation, respectively (Figure 1C). The migration angle was defined as $\tan^{-1}(\frac{Y2-Y1}{X2-x1})$. Using the migration distance and orientation, we obtained a migration plot for each, which could be depicted in a polar coordinate system, as shown in Figure 1 (D-F). The anode in the polar plots of DC stimulated experiments is located at 180°angle, Figure 1 (E,F). For better comparison of all experi-

ments, we binned the migration angles in 36 sectors of 10º each, and classified migration speeds in a scoring system. Thus, the migration angle was calculated starting from the original cell position, and angles were assigned to the 36 sectors, where sector 10-18 (90-180°) and 18–26 (180-270°) represent anode-directed migration, while sectors 1-9 and 27-36 (0-90 and 270 to 360 °) represent cathode-directed cell migration. To construct polar plots (Figure 1 D-E) illustrating both migration direction and velocity, the migration speed of single cells was colour coded from 0 to 18 µm/h in 9 groups of 3 µm/h bins. The relative sector lengths denote the percentage of cells migrating at a certain speed range.

## Acknowledgments

This study was funded by CRC 1270 ELAINE, projects C03, C02 and A02 (RK, RB and UvR). We thank Ms. Doris Hansmann for providing the primary human osteoblasts.

## References

**Barton DL**, Henkes S, Weijer CJ, Sknepnek R. Active Vertex Model for cell-resolution description of epithelial tissue mechanics. PLoS Computational Biology. 2017; doi: 10.1371/journal.pcbi.1005569.

**Bhattacharya K**, Vicsek T. Collective decision making in cohesive flocks. New Journal of Physics. 2010; doi: 10.1088/1367-2630/12/9/093019.

**Bi D**, Yang X, Marchetti MC, Manning ML. Motility-driven glass and jamming transitions in biological tissues. Physical Review X. 2016; doi: 10.1103/PhysRevX.6.021011.

**Bittig AT**, Jeschke M, Uhrmacher AM. Towards modelling and simulation of crowded environments in cell biology. In: *AIP Conference Proceedings*; 2010. doi: 10.1063/1.3497964.

**Brighton CT**, Hozack WJ, Brager MD, Windsor RE, Pollack SR, Vreslovic EJ, Kotwick JE. Fracture healing in the rabbit fibula when subjected to various capacitively coupled electrical fields. Journal of Orthopaedic Research. 1985; 3(3):331–340. doi: 10.1002/jor.1100030310.

**Brugués A**, Anon E, Conte V, Veldhuis JH, Gupta M, Colombelli J, Muñoz JJ, Brodland GW, Ladoux B, Trepat X. Forces driving epithelial wound healing. Nature Physics. 2014; doi: 10.1038/NPHYS3040.

**Cho Y**, Son M, Jeong H, Shin JH. Electric field-induced migration and intercellular stress alignment in a collective epithelial monolayer. Molecular Biology of the Cell. 2018; doi: 10.1091/mbc.E18-01-0077.

**Ferrier J**, Ross SM, Kanehisa J, Aubin JE. Osteoclasts and osteoblasts migrate in opposite directions in response to a constant electrical field. JCell Physiol. 1986 dec; 129(0021-9541 (Linking)):283–288.

**Gruler H**, Nuccitelli R. The Galvanotaxis response mechanism of keratinocytes can be modeled as a proportional controller. Cell Biochemistry and Biophysics. 2000; doi: 10.1385/cbb:33:1:33.

**Guido I**, Diehl D, Olszok NA, Bodenschatz E. Cellular velocity, electrical persistence and sensing in developed and vegetative cells during electrotaxis. PLoS ONE. 2020; doi: 10.1371/journal.pone.0239379.

**Hart FX**, Palisano JR. Glycocalyx bending by an electric field increases cell motility. Bioelectromagnetics. 2017; doi: 10.1002/bem.22060.

**Henkes S**, Kostanjevec K, Collinson JM, Sknepnek R, Bertin E. Dense active matter model of motion patterns in confluent cell monolayers. Nature Communications. 2020; doi: 10.1038/s41467-020-15164-5.

**Hiemer B**, Ziebart J, Jonitz-Heincke A, Grunert PC, Su Y, Hansmann D, Bader R. Magnetically induced electrostimulation of human osteoblasts results in enhanced cell viability and osteogenic differentiation. International Journal of Molecular Medicine. 2016 jul; 38(1):57–64. doi: 10.3892/ijmm.2016.2590.

**Jacobs DJ**, Trivedi D, David C, Yengo CM. Kinetics and thermodynamics of the rate-limiting conformational change in the actomyosin V mechanochemical cycle. J MolBiol. 2011 apr; 407(0022-2836 (Linking)):716–730.

**Jhawar J**, Morris RG, Amith-Kumar UR, Danny Raj M, Rogers T, Rajendran H, Guttal V. Noise-induced schooling of fish. Nature Physics. 2020; doi: 10.1038/s41567-020-0787-y.

**Kaivosoja E**, Sariola V, Chen Y, Konttinen YT. The effect of pulsed electromagnetic fields and dehydroepiandrosterone on viability and osteo-induction of human mesenchymal stem cells. Journal of Tissue Engineering and Regenerative Medicine. 2015 jan; 9(1):31–40. doi: 10.1002/term.1612.

**Lara Rodriguez L**, Schneider IC, Directed cell migration in multi-cue environments; 2013. doi: 10.1039/c3ib40137e.

**Liang Y**, Tian H, Liu J, Lv YL, Wang Y, Zhang JP, Huang YS. Application of stable continuous external electric field promotes wound healing in pig wound model. Bioelectrochemistry. 2020; doi: 10.1016/j.bioelechem.2020.107578.

**Lin BJ**, Tsao SH, Chen A, Hu SK, Chao L, Chao PHG. Lipid rafts sense and direct electric field-induced migration. Proceedings of the National Academy of Sciences of the United States of America. 2017; doi: 10.1073/pnas.1702526114.

**Lochner K**, Fritsche A, Jonitz A, Hansmann D, Mueller P, Mueller-Hilke B, Bader R. The potential role of human osteoblasts for periprosthetic osteolysis following exposure to wear particles. International Journal of Molecular Medicine. 2011; doi: 10.3892/ijmm.2011.778.

**Merkel M**, Manning ML, Using cell deformation and motion to predict forces and collective behavior in morphogenesis; 2017. doi: 10.1016/j.semcdb.2016.07.029.

**Piotrowski-Daspit ASA**. Physical Forces and Collective Cell Migration in Development and Disease. PhD thesis; 2016.

**Rohde M**, Ziebart J, Kirschstein T, Sellmann T, Porath K, Kühl F, Delenda B, Bahls C, van Rienen U, Bader R, Köhling R. Human Osteoblast Migration in DC Electrical Fields Depends on Store Operated Ca2+-Release and Is Correlated to Upregulation of Stretch-Activated TRPM7 Channels. Frontiers in Bioengineering and Biotechnology. 2019; doi: 10.3389/fbioe.2019.00422.

**Saltukoglu D**, Grünewald J, Strohmeyer N, Bensch R, Ulbrich MH, Ronneberger O, Simons M. Spontaneous and electric feld-controlled front-rear polarization of human keratinocytes. Molecular Biology of the Cell. 2015; doi: 10.1091/mbc.E14-12-1580.

**Sato MJ**, Kuwayama H, Van Egmond WN, Takayama ALK, Takagi H, Van Haastert PJM, Yanagida T, Ueda M. Switching direction in electric-signal-induced cell migration by cyclic guanosine monophosphate and phosphatidylinositol signaling. Proceedings of the National Academy of Sciences of the United States of America. 2009; doi: 10.1073/pnas.0809974106.

**Schienbein M**, Gruler H. Langevin equation, Fokker-Planck equation and cell migration. Bulletin of Mathematical Biology. 1993; doi: 10.1007/BF02460652.

**Sich NM**, O'Donnell TJ, Coulter SA, John OA, Carter MS, Cremo CR, Baker JE. Effects of actin-myosin kinetics on the calcium sensitivity of regulated thin filaments. J BiolChem. 2010 dec; 285(0021-9258 (Linking)):39150–39159.

**Simpson MJ**, Lo KY, Sun YS. Quantifying the roles of random motility and directed motility using advection-diffusion theory for a 3T3 fibroblast cell migration assay stimulated with an electric field. BMC Systems Biology. 2017; doi: 10.1186/s12918-017-0413-5.

**Stains JP**, Civitelli R, Cell-to-cell interactions in bone; 2005. doi: 10.1016/j.bbrc.2004.11.078.

**Stains JP**, Fontana F, Civitelli R. Intercellular junctions and cell-cell communication in the skeletal system. In: *Principles of Bone Biology*; 2019.doi: 10.1016/B978-0-12-814841-9.00018-X.

**Szabó B**, Szöllösi GJ, Gönci B, Jurányi Z, Selmeczi D, Vicsek T. Phase transition in the collective migration of tissue cells: Experiment and model. Physical Review E - Statistical, Nonlinear, and Soft Matter Physics. 2006; doi: 10.1103/PhysRevE.74.061908.

**Tai G**, Reid B, Cao L, Zhao M. Electrotaxis and wound healing: experimental methods to study electric fields as a directional signal for cell migration. Methods in molecular biology (Clifton, NJ). 2009; doi: 10.1007/978-1-60761-198-1_5.

**Thurley K**, Wu LF, Altschuler SJ. Modeling Cell-to-Cell Communication Networks Using Response-Time Distributions. Cell Systems. 2018; doi: 10.1016/j.cels.2018.01.016.

**Trepat X**, Wasserman MR, Angelini TE, Millet E, Weitz DA, Butler JP, Fredberg JJ. Physical forces during collective cell migration. Nature Physics. 2009; doi: 10.1038/nphys1269.

**Vanegas-Acosta JC**, Garzón-Alvarado DA, Zwamborn APM. Mathematical model of electrotaxis in osteoblastic cells. Bioelectrochemistry. 2012; doi: 10.1016/j.bioelechem.2012.08.002.

**Vicsek T**, Czirk A, Ben-Jacob E, Cohen I, Shochet O. Novel type of phase transition in a system of self-driven particles. Physical Review Letters. 1995; doi: 10.1103/PhysRevLett.75.1226.

**Waters CM**, Bassler BL, Quorum sensing: Cell-to-cell communication in bacteria; 2005. doi: 10.1146/annurev.cellbio.21.012704.131001.

**Wu D**, Lin F. A receptor-electromigration-based model for cellular electrotactic sensing and migration. Biochemical and Biophysical Research Communications. 2011; doi: 10.1016/j.bbrc.2011.07.004.

**Zajdel TJ**, Shim G, Wang L, Rossello-Martinez A, Cohen DJ. SCHEEPDOG: Programming Electric Cues to Dynamically Herd Large-Scale Cell Migration. Cell Systems. 2020; doi: 10.1016/j.cels.2020.05.009.

**Zhao M**, Pu J, Forrester JV, McCaig CD. Membrane lipids, EGF receptors, and intracellular signals colocalize and are polarized in epithelial cells moving directionally in a physiological electric field. The FASEB journal : official publication of the Federation of American Societies for Experimental Biology. 2002; doi: 10.1096/fj.01-0811fje.

**Zhao Z**, Watt C, Karystinou A, Roelofs AJ, McCaig CD, Gibson IR, De Bari C. Directed migration of human bone marrow mesenchymal stem cells in a physiological direct current electric field. European Cells and Materials. 2011; doi: 10.22203/eCM.v022a26.

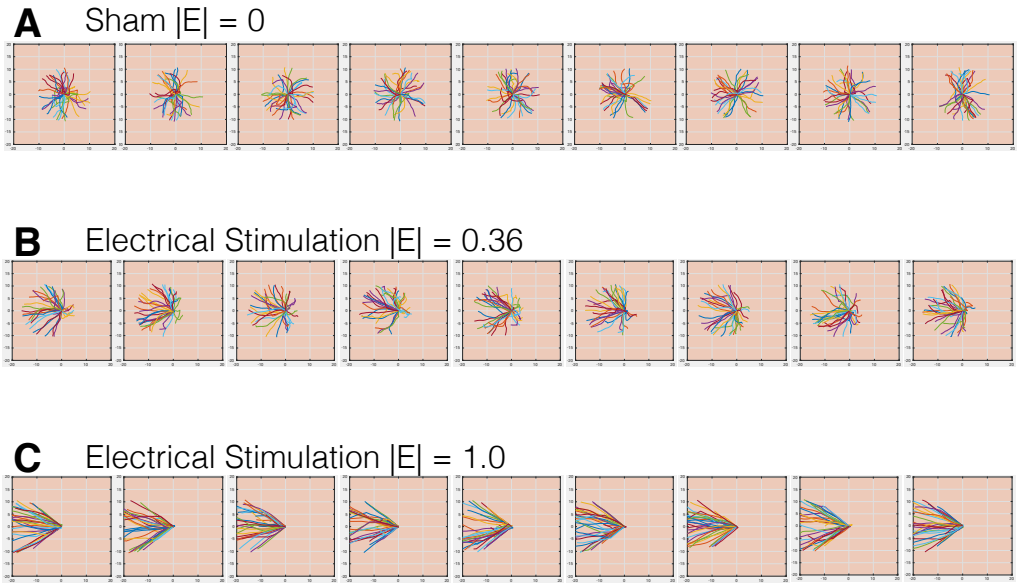


**Figure 3–Figure supplement 1.** Simulation results of ten separate simulation runs in the case of (**A**) no electrical stimulation, which corresponds to experimental sham, (**B**) stimulation with electrical field amplitude of 0.36, which corresponds to the experimental field stimulation strength of 160 V/m, and, (**C**) stimulation with electrical field amplitude of 1, which corresponds to the experimental field stimulation strength of 436 V/m.